Absolute Stability Analysis Using the Liénard Equation: A Study Derived From Control of Fuel Cell Ultracapacitor Hybrids

William Nowak
Rochester Institute of Technology,
Rochester, NY 14623

Daniel Geiyer
Department of Mechanical and Aerospace Engineering,
University of Central Florida,
Orlando, FL 32816

Tuhin Das[1]
Department of Mechanical and Aerospace Engineering,
University of Central Florida,
Orlando, FL 32816
e-mail: Tuhin.Das@ucf.edu

Load-following in solid oxide fuel cells (SOFCs), hybridized with an ultracapacitor for energy storage, refers to an operating mode where the fuel cell's generated power follows the variable power demand, delivering the total demanded power at steady-state. Implementing this operating mode presents a rich set of problems in dynamical systems and control. This paper focuses on state-of-charge (SOC) control of the ultracapacitor during load-following, under transient constraints, and in the presence of an unknown nonlinearity. The problem is generalized to stabilization of a plant containing a cascaded connection of a driver and a driven dynamics, where the former is nonlinear and largely unknown. Closed-loop stability of the system is studied as a Lur'e problem and via energy-based Lyapunov equations, but both impose conservative conditions on the nonlinearity. An alternate approach is developed, where the closed-loop dynamics are formulated as a class of Liénard equations. The corresponding analysis, which is based on the nonlinear characteristics of the Liénard equation, yields more definitive and less conservative stability criteria. Additional conditions that lead to limit cycles are also derived, and a bifurcation pattern is revealed. The generality of the proposed approach indicates applicability to a variety of nonlinear systems. [DOI: 10.1115/1.4032318]

1 Introduction

Solid oxide fuel cells are electrochemical energy conversion devices that offer advantages such as high efficiency, fuel flexibility, tolerance to fuel impurities, and internal reforming capability without the need of precious metal catalysts [1]. However, operating them in load-following mode while preventing fuel starvation can pose a number of challenges. The SOFCs are susceptible to irreversible damages caused by fuel starvation, especially at high efficiency operating points (i.e., at high fuel utilization, between 70% and 90% [2–4]). The starvation problem can be quite effectively alleviated by regulating the fuel cell current on the basis of actual fuel flow [5,6], which is lagged by the fuel supply system (FSS) of the SOFC. This approach has the advantage of not relying on accurate mathematical models which can be cumbersome and system specific. However, current regulation causes a mismatch between the demanded and delivered power. To compensate for this mismatch and achieve accurate load-following, the SOFC is hybridized with an ultracapacitor. The ultracapacitor serves to either absorb or inject power-bursts during transient situations. The fuel cell concurrently modulates its own power generation to maintain the ultracapacitor's SOC at a healthy level. Thus, control strategies are needed to stabilize this hybrid fuel cell ultracapacitor system [6,7].

One challenge of the aforementioned scenario is SOC control of the ultracapacitor in the presence of unknown and nonlinear dynamics of the FSS. Specifically, the FSS dynamics and the SOC dynamics form a cascaded connection, where the former is the driver and the latter is driven. The problem is abstracted and posed in a generalized theoretical form. Thereafter for a given simple feedback controller, we determine how closed-loop stability is impacted by different nonlinearities, which can be categorized for instance by sector conditions. While traditional approaches such as absolute stability or energy-based Lyapunov functions are applicable [8], the resulting stability conditions are conservative. To this end, the closed-loop dynamics are expressed as a class of Liénard equations [9,10], and their nonlinear characteristics are used for stability analysis.

The Liénard equation refers to a category of nonlinear differential equations where existence of limit cycles is proven under additional conditions. Following the established analytical foundation of Liénard equations, we prove that our specific equation transitions from a stable equilibrium to a stable limit cycle, and the existence of a bifurcation pattern is shown. The stability predictions made by the proposed method are less conservative and provide greater resolution into the nature of the equilibrium (i.e., stable equilibrium versus stable limit cycle) than those obtained using absolute stability. The results are also indicative of a greater flexibility in designing closed-loop control to achieve a stable equilibrium than that predicted by absolute stability methods. Finally, the proposed approach is extended to incorporate parameter uncertainties and local stability conditions are derived.

The paper is organized as follows: We first describe the hybrid SOFC system which is the basis of this work. The feedback structure consisting of the cascaded configuration is developed and the stability problem is formally stated. Next, the problem is addressed using traditional methods such as the *Circle Criterion* and conventional Lyapunov analysis. The Liénard system formulation is presented next and a number of new stability results are proven. Finally, the approach is extended to incorporate parameter uncertainties and preliminary results are provided. Over the paper, analysis is accompanied by simulations. Finally, conclusions and acknowledgments are stated and references are listed.

2 Background and Problem Formulation

2.1 Reformer-Based SOFC and Ultracapacitor System. In this section, we present a brief background of the hybrid fuel cell energy system and discuss the associated control problems. A

[1]Corresponding author.

Contributed by the Dynamic Systems Division of ASME for publication in the Journal of Dynamic Systems, Measurement, and Control. Manuscript received April 4, 2015; final manuscript received December 9, 2015; published online January 12, 2016. Assoc. Editor: Junmin Wang.

schematic of the hybrid SOFC system is shown in Fig. 1 [11]. The system consists of a fuel cell and an ultracapacitor that are connected in parallel to an electrical bus through direct current (DC)/DC converters C_1 and C_2, respectively. Details of operation of the reformer-based SOFC system can be found in Refs. [6] and [11]. In summary, the reformer reforms the fuel, methane with flow rate of $\dot{N}_f$, to a hydrogen rich gas mixture that is used by the SOFC to deliver the current i_{fc}. The SOFC generates a steam-rich gas mixture as a byproduct of current draw, a fraction (k_c) of which is recirculated to the reformer for providing steam for reforming. The converter C_1 provides unidirectional power flow and draws current i_{fc} from the fuel cell, as commanded by the controller. C_2 is a bidirectional DC/DC converter that maintains a constant bus voltage V_L. The efficiencies of the converters C_1 and C_2 are represented as η_1 and η_2. It is also assumed that measurements of the fuel cell voltage V_{fc}, ultracapacitor voltage V_{uc}, load current i_L, and actual fuel flow $\dot{N}_f$ are available to the controller. The variables V_{fc}, V_{uc}, and i_L are readily measurable, and the measurement of $\dot{N}_f$ is available in the FSS systems consisting of a fuel pump and/or valve. Hence, it is reasonable to assume availability of these signals for control implementation. The controller generates two command signals, namely, the demanded fuel flow $\dot{N}_{f,d}$ and i_{fc}. The general electrical power balance equation, as evident from the system schematic, is expressed as

$$V_L i_L = \eta_1 V_{\text{fc}} i_{\text{fc}} + \eta_2 V_{\text{uc}} i_{\text{uc}} \tag{1}$$

The fuel cell is operated in a load-following mode. In this mode, the demanded fuel cell current $i_{\text{fc},d}$ is primarily based on the net power requirement $V_L i_L$ with deviations to account for excess/deficient SOC of the ultracapacitor. The formulation of $i_{\text{fc},d}$ is

$$i_{\text{fc},d} = \frac{V_L i_L}{\eta_1 V_{\text{fc}}} - kE_s, \quad \text{where,} \quad E_s = S - S_t \quad \text{and}$$
$$S = \frac{V_{\text{uc}}}{V_{\max}}, \quad S_t = \frac{V_{\text{uc},t}}{V_{\max}} \tag{2}$$

where S is the instantaneous SOC of the ultracapacitor, S_t and $V_{\text{uc},t}$ are the target SOC and target voltage, respectively, $V_{\max}$ is the maximum ultracapacitor voltage, and $k>0$ is a controller gain. Thus, the first term in Eq. (2) implements load-following while the latter term provides the perturbations in the fuel cell power needed to maintain the SOC at the target S_t. Specifically, the second term is active only during transients and is zero at steady-state. The first term is always active and it ensures that the power demand is completely met by the fuel cell at steady-state.

For SOFCs, the dynamic limitations in load-following are manifested in the transient response of fuel utilization U. Fuel utilization is defined as the ratio of hydrogen consumption to the net available hydrogen in the anode [2]. Typically, $80-90\%$ is set as the target range ([2,12]) for optimal efficiency. Constant fuel utilization (U) is a primary mode of operation of SOFCs [13–16]. In the constant fuel utilization mode, the fuel flow is varied in conjunction with changes in power demand, to maintain U at a set-point ($\approx$85%). However, SOFCs can be prone to hydrogen starvation at U values of $80-90\%$ due to delays in the FSS (shown in Fig. 1). This is especially true under transients in power demand. Fuel starvation can be prevented by transient control of U. However, direct measurement of U is intrusive and expensive, and observer-based estimation is computation intensive [6,7]. To achieve this transient control in a practical manner, the controller in Fig. 1 implements a current regulation strategy, depicted in Fig. 1. The strategy manipulates i_{fc} based on the actual fuel flow $\dot{N}_f$, while commanding a target fuel flow $\dot{N}_{f,d}$ that is based on the demanded current $i_{\text{fc},d}$. In doing so, a simple method for transient control of U is achieved, as explained next. The method uses an analytical equation relating U, fuel flow, and current draw in steady-state. For the SOFC system of interest, the steady-state expression of U has the form [6,11]

$$U = \frac{1-k_c}{\left(4nF\dot{N}_f / i_{\text{fc}} \mathcal{N}_{\text{cell}}\right) - k_c} \tag{3}$$

where i_{fc} is the fuel cell current, $\dot{N}_f$ is the fuel flow rate, $\mathcal{N}_{\text{cell}}$ is the number of cells in series, $F=96{,}485.34$ Coul/mol is Faraday's constant, $n=2$ is the number of electrons involved in each electrochemical reaction, and k_c is the constant recirculation fraction. Equation (3) is rearranged such that a demanded fuel flow $\dot{N}_{f,d}$ can be calculated given $i_{\text{fc},d}$ and a target U_{ss}

$$\dot{N}_{f,d} = \frac{i_{\text{fc},d}\mathcal{N}_{\text{cell}}}{4nFU_{\text{ss}}}[1-(1-U_{\text{ss}})k_c] \quad \Rightarrow \quad \dot{N}_{f,d} = \sigma i_{\text{fc},d} \tag{4}$$

where $\sigma = \mathcal{N}_{\text{cell}}[1-(1-U_{\text{ss}})k_c]/4nFU_{\text{ss}}$. It is also noted that the dynamics of the FSS are considered unknown and nonlinear, and is represented by

$$\frac{d\dot{N}_f}{dt} = g\left(\dot{N}_f, \dot{N}_{f,d}\right), \quad \text{and} \quad \frac{d\dot{N}_f}{dt} = 0 \Rightarrow \dot{N}_f = \dot{N}_{f,d} \tag{5}$$

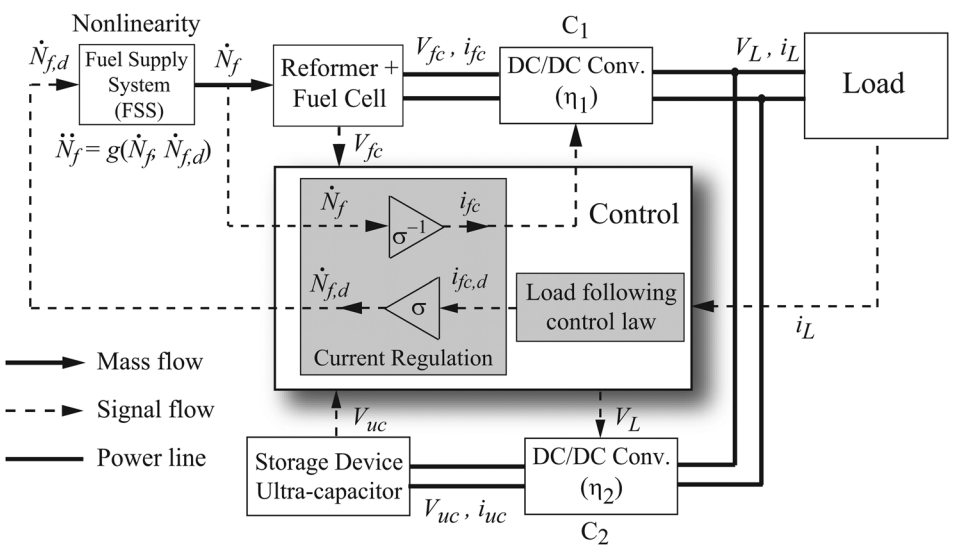

Fig. 1 Schematic diagram of the hybrid SOFC system

Equation (3) is manipulated to compensate for delays along the fuel supply path by regulating current drawn from the system, based on actual fuel flow, i.e.,

$$i_{\text{fc}} = \frac{4nFU_{\text{ss}}\dot{N}_f}{\mathcal{N}_{\text{cell}}}\frac{1}{[1-(1-U_{\text{ss}})k_c]} \quad \Rightarrow \quad i_{\text{fc}} = \sigma^{-1}\dot{N}_f \tag{6}$$

Next, we develop the equations of the overall feedback system shown in Fig. 1 by incorporating the dynamic equation of the ultracapacitor. Thereafter, we generalize the feedback control structure for further analysis.

2.2 Cascaded Configuration and the Generalized Feedback Structure. From Eq. (2) and using the standard capacitor equation, we get

$$\left.\begin{aligned} \dot{V}_{\text{uc}} &= -i_{\text{uc}}/C \\ \dot{E}_s = \dot{S} &= \dot{V}_{\text{uc}}/V_{\max} \end{aligned}\right\} \quad \Rightarrow \quad \dot{E}_s = -\frac{i_{\text{uc}}}{CV_{\max}} \tag{7}$$

From Eqs. (1) and (7) we have

$$\dot{E}_s = -\left(\frac{1}{CV_{\max}}\right)\left[\left(\frac{V_L i_L}{\eta_2 V_{\text{uc}}}\right) - \left(\frac{\eta_1 V_{\text{fc}}}{\eta_2 V_{\text{uc}}}\right) i_{\text{fc}}\right] \tag{8}$$

From Fig. 1 and Eqs. (4)–(6), the nonlinear dynamics of the FSS are expressed as

$$\begin{aligned} &\frac{di_{\text{fc}}}{dt} = \sigma^{-1} g(\sigma i_{\text{fc}}, \sigma i_{\text{fc},d}) = f(i_{\text{fc}}, i_{\text{fc},d}), \quad \text{and} \\ &\frac{di_{\text{fc}}}{dt} = 0 \Rightarrow i_{\text{fc}} = i_{\text{fc},d} \end{aligned} \tag{9}$$

Thus, from Eqs. (8) and (9), we note that the dynamic equations of E_s and i_{fc} are effectively in a cascaded connection. This connection, along with the load-following control law of Eq. (2), is shown in Fig. 2. The cascaded system consists of the unknown FSS dynamics acting as a driver system and the SOC dynamics acting as the driven system. It can be verified that the closed-loop system of Fig. 2 has a unique equilibrium at $i_{\text{fc}} = i_{\text{fc},d} = V_L i_L/(\eta_1 V_{\text{fc}}), E_s = 0$. This ensures that the closed-loop system addresses load-following and regulation of the ultracapacitor's SOC simultaneously.

Since a generalized treatment is the goal of this paper, the system in Fig. 2 is expressed as shown in Fig. 3. The mapping between the variables of Figs. 3 and 2 is

$$\begin{aligned} &y \equiv i_{\text{fc}}, \quad r \equiv i_{\text{fc},d}, \quad x \equiv E_s, \quad \dot{x} = h_1 + h_2 y, \\ &h_1 \equiv -\frac{1}{\eta_2}\left(\frac{V_L i_L}{CV_{\max}V_{\text{uc}}}\right), \quad h_2 \equiv \frac{\eta_1}{\eta_2}\left(\frac{V_{\text{fc}}}{CV_{\max}V_{\text{uc}}}\right) \end{aligned} \tag{10}$$

In the ensuing analysis, we make the following assumptions:

(1) The unknown nonlinear function $f(y, r)$, similar to Eq. (9), satisfies

$$\dot{y} = f(y,r), \quad \text{such that} \quad \dot{y} \to 0 \Rightarrow e \triangleq (y-r) \to 0 \tag{11}$$

The latter condition imposes a zero steady-state error between y and the reference signal r. We assume that this zero steady-state error simplifies the nonlinearity to

$$f(y,r) = -f(y-r) \equiv -f(e), \quad \Rightarrow \quad \dot{y} = -f(e) \quad \text{and} \quad f(0) = 0 \tag{12}$$

Equation (12) is not restrictive. Commonly occurring characteristics such as ramped, rate-limited, or saturation-based dynamics fall within this category, as shown in Ref. [7].

(2) In Eq. (10), we treat h_1 and h_2 as known constants. Hence, the control law of Eq. (2) maps to

$$r = -\frac{h_1}{h_2} - kx, \quad k > 0 \tag{13}$$

We note that assuming h_1 and h_2 as constants imposes the driven system to be linear time invariant (LTI) in the generalized analysis. In Sec. 5, the restriction of h_1 and h_2 being known constants will be relaxed to unknown constants. The validity of assuming h_1 and h_2 as constants for the SOFC system specifically will be discussed in Sec. 5.3.

This completes the description of the generalized feedback system. Next we present the problem statement and summarize the approach adopted in our earlier works. The discussion motivates the approach presented in this paper.

2.3 Problem Statement and Prior Approach to Stability Analysis. The problem statement is as follows:

Problem Statement: Given the feedback system of Fig. 3 with the unknown nonlinear function $f(y,r) = -f(e)$ as given in Eq. (12), determine conditions on $f(e)$ or category of functions $f(e)$, which yield a stable or an unstable equilibrium at $[x, e]^{\text{T}} = [0, 0]^{\text{T}}$, or generate a limit cycle.

In our earlier works, namely [6,7], the aforementioned stability analysis was conducted under certain assumptions on the time-domain characteristics of the nonlinear dynamics of Eq. (12), i.e., $\dot{y} = -f(e)$. To outline this approach, we first derive the following from Eqs. (10) and (13):

$$\dot{x} = h_1 + h_2 y = h_1 + h_2(e+r) = -h_2 kx + h_2 e \tag{14}$$

Then, if we assume e to satisfy a general exponential decay condition

$$|e(t)| \le \gamma |e(t_0)|\, e^{-\zeta(t-t_0)}, \forall |e(t_0)| < r_0 \tag{15}$$

then it can be proven using Eqs. (14) and (15) that the origin of $[x,\ e]^{\text{T}}$ is also exponentially stable. Details and proof of this result under additional practical considerations can be found in Ref. [6]. Furthermore, if $|e(t)|$ is assumed to be bounded, then the system in Eq. (14) with e as the input can be shown to be input-to-state stable (ISS, Ref. [8]). This is also established in detail in Ref. [6]. Assuming time-domain characteristics is one way to overcome the issue of unknown nonlinearity. However, this approach has the following shortcomings:

(1) The time-domain characteristic of y is dependent on the nonlinear function $f(e)$. Hence, a more fundamental approach to stability analysis is to derive conditions on $f(e)$

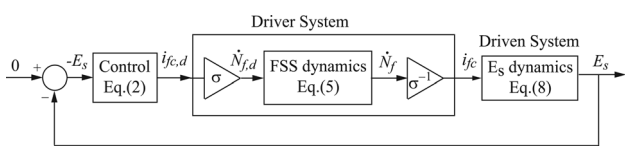

Fig. 2 SOFC/UC hybrid as a cascaded system

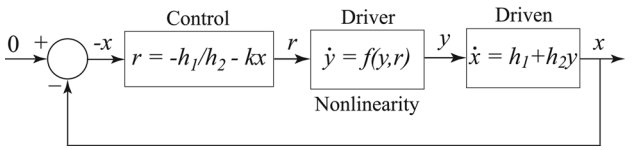

Fig. 3 Generalized form of Fig. 2

directly, and understand the performance limitations of the controller in Eq. (13) for classes of nonlinearities.

(2) Assuming a time domain characteristic allows us to analyze stability of x in isolation, treating e as an external input in Eq. (14). However, our system of interest, i.e., Fig. 3, is inherently a closed-loop system. Hence, in terms of stability analysis, the coupled dynamics of e and x must be considered as a whole.

Both limitations will be addressed with the stability analysis approach presented in Sec. 3.

3 Stability Analysis

In this section, we first derive the coupled state equations. Subsequently, we formulate the stability problem as a classical *absolute stability problem* [8,17], and derive sector conditions on $f(e)$. Thereafter, we carry out analysis using an energy-based Lyapunov function. Although both methods yield sufficient stability-conditions applied to $f(e)$, they are conservative. In Sec. 4, we show that improved stability predictions can be made by applying results from nonlinear dynamics.

3.1 Coupled Dynamics With Unknown Nonlinearity. To derive the coupled closed-loop equation, we observe from Eqs. (11), (13), and (14) that

$$\begin{aligned}\dot{y} &= \dot{e} + \dot{r} = f(y,r) = -f(e) \Rightarrow \dot{e} = -f(e) + k\dot{x} \\ &= -f(e) + kh_2 e - h_2 k^2 x\end{aligned} \tag{16}$$

Thus, the closed-loop dynamic equations are

$$\dot{x} = -h_2 kx + h_2 e, \quad \dot{e} = -f(e) + kh_2 e - h_2 k^2 x \tag{17}$$

Applying the following coordinate transform:

$$z = e - kx \tag{18}$$

Equation (17) can be written as

$$\dot{z} = -f(e), \quad \dot{e} = -f(e) + kh_2 z \tag{19}$$

Equation (19) represents the coupled dynamics of e and z or equivalently e and x, since x relates to e and z per Eq. (18). In carrying out a stability analysis of this system, the obvious issue is the lack of knowledge of the function $f(e)$. We first note that the system in Eq. (19) has equilibria in the state-space at $f(e) = 0$ and $z = 0$. The specific equilibrium point of interest is the origin $z = e = 0$ since, from Eq. (13), it corresponds to the state where $x = 0$, which is the objective of our control design. The existence of this equilibrium point is guaranteed by imposing the condition $f(0) = 0$ in Eq. (12). Our approach will be to consider classes of nonlinear functions $f(e)$ and to investigate their impact on the stability of the aforementioned origin of the state-space.

3.2 Lur'e Problem Formulation and Absolute Stability. Stability of the origin of Eq. (19) can be analyzed as a Lur'e problem [8,17]. The Lur'e problem considers the stability of an interconnection between a LTI system with a memoryless nonlinearity. In formulating this problem, we express Eq. (19) as

$$\begin{bmatrix}\dot{z}\\ \dot{e}\end{bmatrix} = \begin{bmatrix}0 & 0\\ kh_2 & 0\end{bmatrix}\begin{bmatrix}z\\ e\end{bmatrix} + \begin{bmatrix}1\\ 1\end{bmatrix}u, \quad Y = \begin{bmatrix}0 & 1\end{bmatrix}\begin{bmatrix}z\\ e\end{bmatrix}, \quad u = -f(e) \tag{20}$$

Thus, the resulting transfer function between u and $Y = e$ is given by

$$\frac{Y(s)}{u(s)} = G(s) = \frac{s + kh_2}{s^2} \tag{21}$$

A premise of the Lur'e problem is that the matrices

$$\mathbf{A} = \begin{bmatrix}0 & 0\\ kh_2 & 0\end{bmatrix}, \quad \mathbf{B} = \begin{bmatrix}1\\ 1\end{bmatrix}, \quad \mathbf{C} = \begin{bmatrix}0 & 1\end{bmatrix} \tag{22}$$

form a controllable pair $(\mathbf{A}, \mathbf{B})$ and an observable pair $(\mathbf{A}, \mathbf{C})$. These conditions are satisfied in Eq. (22). Next, it can be verified that the system of Eq. (19) can be considered as an interconnection of a linear and a nonlinear component, as shown in Fig. 4. The structure in Fig. 4 is mathematically equivalent to the system representation of Fig. 3.

The above formulation conforms to the structure of the Lur'e problem. Thereby, it allows direct application of the *Circle Criterion* [8,17] to obtain a sector condition on $f(e)$ that will ensure stability of the feedback system in Fig. 4. From Theorem 7.1 of Ref. [8], we observe that the sector condition $\psi \in [K_1, K_2]$, where $K_2 > K_1 > 0$, will guarantee absolute stability of the origin of the feedback system, if $D(s) = [I + K_2 G(s)].[I + K_1 G(s)]^{-1}$ is strictly positive real (SPR). From *Theorem 7.1* of Ref. [18], note that $D(s)$ is SPR if it is strictly stable and $\mathrm{Re}(D(j\omega)) \geq 0 \; \forall \; \omega > 0$. The transfer function $D(s)$ takes the form

$$D(s) = \frac{[I + K_2 G(s)]}{[I + K_1 G(s)]} = \frac{s^2 + K_2 s + K_2 kh_2}{s^2 + K_1 s + K_1 kh_2} \tag{23}$$

It can be verified that for stability, the necessary and sufficient conditions are $K_1 > 0$ and $K_1 kh_2 > 0$. This effectively means $K_1 > 0$ and $k > 0$ must be satisfied. From Eq. (23), the requirement $\mathrm{Re}(D(j\omega)) \geq 0$ reduces to the inequality condition

$$\omega^4 + (K_1 K_2 - kh_2 K_1 - kh_2 K_2)\omega^2 + k^2 h_2^2 K_1 K_2 > 0 \quad \forall \omega > 0 \tag{24}$$

We explore the sector conditions at two extremities, namely, $K_1 \to 0$ and $K_2 \to \infty$, while maintaining $K_2 > K_1 > 0$. When $K_1 \to 0$, Eq. (24) requires $(kh_2 K_2) < 0$, which is not feasible since $K_2 > 0$, $h_2 > 0$ and we must have the controller gain $k > 0$ for stability. When the latter scenario is valid, i.e., $K_2 \to \infty$, Eq. (24) requires $(K_1 - kh_2) > 0$, which is feasible. Thus, the sector condition on $f(e)$ for stability is $\psi \in [kh_2, \infty]$, and it is dependent on the controller gain k. Intuitively this interdependence is expected since the nonlinear dynamics should have an impact on the choice of the gain k. The *circle criterion* provides a quantitative relation that can be exploited to guarantee stability. In addition to the condition $\psi \in [kh_2, \infty]$, other sector conditions may also be derived from Eq. (24). Using the quadratic form of Eq. (24), it is clear that the inequality is satisfied for all $\omega > 0$ whenever

$$\begin{aligned}&(K_1 K_2 - kh_2 K_1 - kh_2 K_2) > 0 \quad \text{or} \\ &\begin{cases}(K_1 K_2 - kh_2 K_1 - kh_2 K_2) < 0 \text{ and} \\ (K_1 K_2 - kh_2 K_1 - kh_2 K_2)^2 < 4k^2 h_2^2 K_1 K_2\end{cases}\end{aligned} \tag{25}$$

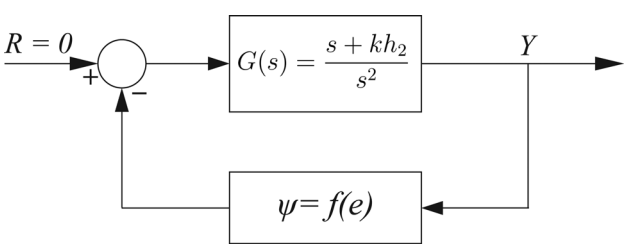

Fig. 4 A Lur'e problem formulation derived from Fig. 3

The above sector-based conditions are sufficient conditions for stability and hence are likely to be conservative. This can be verified by graphically implementing the circle criterion using the Nyquist plot of $G(s)$. In addition, the following simulations also demonstrate the same. In Fig. 5(*a*), the shaded region represents the sector where the circle criterion predicts absolute stability for the feedback system in Fig. 4, with $kh_2 = 0.5$. The function $f_b(e) = 2e$ satisfies the criterion while $f_c(e) = 0.2e$ does not. Although the functions are linear in these simulations, the results are still relevant for checking the conservative nature of circle criterion. The phase-portraits in Figs. 5(*b*) and 5(*c*) were generated for the feedback system of Eq. (19) with functions f_b and f_c, respectively. Finally, we note that instead of considering different functions $f(e)$, we could have equivalently considered different values of the gain k for a fixed $f(e)$ and made similar observations. Next, we explore a Lyapunov-based stability approach for the system.

3.3 Stability Analysis With an Energy-Based Lyapunov Function. In contrast to the absolute stability approach of Sec. 3.2, an energy-based Lyapunov stability analysis gives an alternate criterion of stability, as discussed in this section. In this regard, eliminating the variable z, the system in Eq. (19) is expressed as the following second-order differential equation:

$$\ddot{e} + \frac{df}{de}\dot{e} + kh_2 f(e) = 0 \tag{26}$$

Equation (26) has the structure of a nonlinear mass–spring–damper with $(df/de)\dot{e}$ and $kh_2 f(e)$ representing damping and spring forces, respectively. Hence, the stored energy is chosen as a Lyapunov function candidate

$$V = \frac{1}{2}\dot{e}^2 + \int_0^e kh_2 f(e)de \tag{27}$$

Here, we assume $f(e)$ to be a passive memoryless function (i.e., lying in the 1st − 3rd quadrant and $f(0) = 0$, Ref. [8]). This will ensure that V is positive definite and radially unbounded. Taking the derivative of Eq. (27) and substituting for $\ddot{e}$ from Eq. (26) results in the following:

$$\begin{aligned}\dot{V} &= \dot{e}\left(-\frac{df}{de}\dot{e} - kh_2 f(e)\right) + kh_2 f(e)\dot{e} \\ &= -\frac{df}{de}\dot{e}^2 \le 0 \quad \text{if} \quad \frac{df}{de} > 0 \ \forall e\end{aligned} \tag{28}$$

If $(df/de) > 0$, then from Eq. (28) $\dot{V}$ can only be concluded to be negative semidefinite. Hence, we apply the Barbashin and Krasovskii theorem (see Corollary 4.2 of Ref. [8]). Considering Eqs. (26) and (28)

$$\dot{V} = 0 \Rightarrow \dot{e} = 0 \Rightarrow \ddot{e} = 0 \Rightarrow f(e) = 0 \Rightarrow e = 0 \tag{29}$$

Therefore, it can be concluded that the origin $e = \dot{e} = 0$ is asymptotically stable provided that

$$\left(\frac{df}{de}\right) > 0 \,\forall\, e \tag{30}$$

Thus, unlike the sector condition derived in Sec. 3.2, the above condition is independent of k and h_2 and has no sector condition. However, this condition is still conservative since it confirms stability only for monotonically increasing $f(e)$, a requirement that was not imposed by the sector condition derived from the circle criterion.

It is noted here that other concepts such as the *small gain theorem* or *passivity* could also be used in analyzing this problem [8,19], but would result in similarly conservative stability criteria. The results of both Secs. 3.2 and 3.3 impose the common condition that *$f(e)$ is a passive memoryless function*. In Sec. 4, *we will retain this general condition but we will derive a more definitive stability condition* by analyzing Eq. (26) as a class of Liénard systems.

4 Analysis as a Class of Liénard Equations

4.1 Asymptotic Stability. The Liénard system refers to the following second-order nonlinear differential equation:

$$\ddot{\mu} + p(\mu)\dot{\mu} + q(\mu) = 0 \tag{31}$$

where $p(\mu)$ and $q(\mu)$ are two continuously differentiable functions of μ [9,10]. The Liénard equation has been studied extensively, especially in the context of oscillating circuits. Under additional conditions on the functions $p(\mu)$ and $q(\mu)$, the Liénard equation has a unique and stable limit cycle. The result is detailed in the following theorem:

THEOREM 1 (Liénard's Theorem). *If the functions $p(\mu)$ and $q(\mu)$ in Eq. (31) are continuous and integrable and satisfy the following additional conditions*:

(1) $p(\mu)$ is an even function, and $q(\mu)$ is an odd function such that $\mu\, q(\mu) > 0$;
(2) The functions

$$P(\mu) = \int_0^\mu p(\mu)d\mu, \quad Q(\mu) = \int_0^\mu q(\mu)d\mu \tag{32}$$

tend toward ∞ as $\mu \to \infty$;
(3) $P(\mu)$ has a single positive zero at $\mu = \mu_0$. In the interval $(0, \mu_0)$, $P(\mu)$ is negative, but for $\mu > \mu_0$, $P(\mu)$ is positive and increases monotonically.

Then, under these conditions there exists a unique periodic solution of Eq. (31).

The system in Eq. (26) conforms to the Liénard equation with μ corresponding to e and $p(e) = df/de$, $q(e) = kh_2 f(e)$, $P(e) = \int_0^e p(e)de$ and $Q(e) = \int_0^e q(e)de$. However, it can be verified that $p(e)$ and $q(e)$ do not satisfy all conditions of Theorem 1. In particular, condition (3) is violated because

$$P(e) = \int_0^e p(e)de = \int_0^e \frac{df}{de}de = \big(f(e) - f(0)\big) = f(e) \tag{33}$$

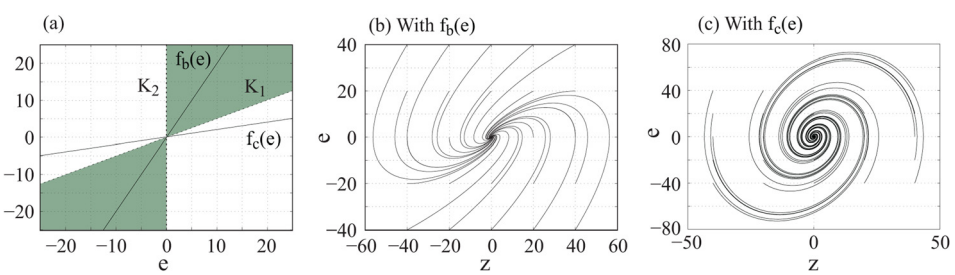

Fig. 5 Circle criterion simulations: (*b*) with $f_b(e)$ and (*c*) with $f_c(e)$

and since $f(e)$ is a passive memoryless function, it cannot have a positive root $e = e_0 > 0$ as required by this condition. Hence, Theorem 1 does not predict a limit cycle solution of Eq. (26). To analyze the stability property of this system, we will use the *Liénard variable* $(\dot{\mu} + P(\mu))$. We note from Eq. (33) that when applied to Eq. (26), the *Liénard variable* takes the form

$$w = \dot{e} + P(e) = \dot{e} + \int_0^e p(e)de = \dot{e} + f(e) \tag{34}$$

This variable is used to study the phase-plane behavior of the Liénard equation in Eq. (31). In Ref. [9], this variable along with the positive definite function

$$V = \frac{1}{2}(\dot{\mu} + P(\mu))^2 + Q(\mu) \tag{35}$$

are used to establish the existence of a limit cycle in the Liénard equation. For the system of interest in Eq. (26), V takes the form

$$V = \frac{1}{2}w^2 + Q(e) = \frac{1}{2}(\dot{e} + f(e))^2 + kh_2\int_0^e f(e)de \tag{36}$$

The function V in Eq. (36) is continuously differentiable, radially unbounded, and positive definite. Hence, it can be treated as a Lyapunov function candidate. The derivative of V along the trajectories of the dynamic equation Eq. (26) is

$$\dot{V} = (\dot{e} + f(e))\left(\ddot{e} + \frac{df}{de}\dot{e}\right) + kh_2 f(e)\dot{e} = -kh_2 f^2(e) \leq 0 \tag{37}$$

The set $\dot{V} = 0$ is satisfied identically only by $f(e) \equiv 0$, i.e., by $e = \dot{e} \equiv 0$. Since the above conditions are true globally, applying the Barbashin and Krasovskii theorem (see Corollary 4.2 of Ref. [8]), we conclude that the origin $e = \dot{e} \equiv 0$ is globally asymptotically stable. In a general sense, we can therefore state the following theorem:

THEOREM 2. *The class of Liénard equation Eq. (31), where $p(\mu) = \alpha(dq/d\mu)$, $q(\mu)$ is a continuously differentiable odd function such that $\mu q(\mu) > 0$, and α is a positive constant, has a globally asymptotically stable equilibrium at the origin $\mu = \dot{\mu} = 0$.*

Proof. The proof is evident from the discussions between Theorems 1 and 2 above, and therefore omitted for the sake of conciseness. ■

Based on the observations above, we state the following corollary:

COROLLARY 1. *The feedback system of Fig. 3 with any unknown nonlinear function $f(y,r) = -f(e)$, which satisfies $f(0) = 0$, and $ef(e) > 0\,\forall\, e \neq 0$, has a globally asymptotically stable equilibrium point at $e = \dot{e} = 0$.*

The result of Corollary 1 is definitive compared to those in Secs. 3.2 and 3.3. This is because it establishes stable closed-loop performance for any passive memoryless function $f(e)$ and for the generic feedback control of Eq. (13), without any additional sector or slope requirements on $f(e)$. Finally, we note from Eq. (17) that the equilibrium $e = \dot{e} = 0$ uniquely corresponds to $x = \dot{x} = 0$.

4.2 Existence of Limit Cycle and Hopf Bifurcation. In this section, we generalize the discussion of Sec. 4.1 and derive

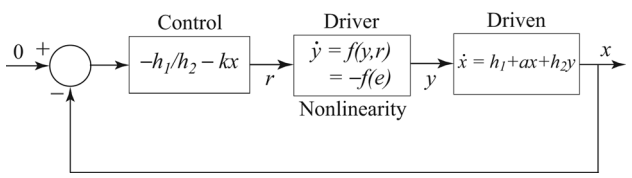

Fig. 6 Feedback system with driven dynamic equation generalized to Eq. (38)

conditions on the feedback system of Fig. 3 under which a limit cycle behavior would emerge. This is a natural step, since the *Liénard's Theorem*, Theorem 1, provides sufficient conditions for existence of limit cycle. For the generalization, we consider the same feedback system as in Fig. 3 with one difference. We generalize the dynamic equation of the driven system to the following:

$$\dot{x} = h_1 + ax + h_2y \tag{38}$$

The modified feedback system with Eq. (38) incorporated is shown in Fig. 6. Replacing the differential equation of x in Eq. (10) with that in Eq. (38) and combining with Eqs. (11) and (13), we get

$$\begin{aligned}\dot{x} &= h_1 + ax + h_2\left(e - \frac{h_1}{h_2} - kx\right)\\ &= -(kh_2 - a)x + h_2e\end{aligned} \tag{39}$$

Noting from Eq. (16) that $\dot{e} = -f(e) + k\dot{x}$, and using Eq. (39) we can write the following dynamic equation for e:

$$\ddot{e} + \left(\frac{df}{de} - a\right)\dot{e} + (kh_2 - a)f(e) = 0 \tag{40}$$

In the analysis, we consider $(kh_2 - a) > 0$, i.e., the feedback gain k is chosen to stabilize the homogeneous dynamics of x. Note that when $a = 0$, Eq. (40) reduces to Eq. (26), which was established by Theorem 2 to have a globally asymptotically stable equilibrium. For nonzero a, we first state the following result:

THEOREM 3. *Consider the feedback system of Fig. 6 where k is chosen such that $(kh_2 - a) > 0$. Let the unknown nonlinear function $f(y,r) = -f(e)$ satisfy $f(0) = 0$, and $ef(e) > 0\,\forall\, e \neq 0$ (i.e., f(e) is a passive memoryless function). Then,*

- If $a \leq 0$, the equilibrium point $\dot{e} = e = 0$ is globally asymptotically stable.
- If $a > 0$, the equilibrium point $\dot{e} = e = 0$ is globally asymptotically stable if f(e) additionally satisfies the sector condition $f(e) \in [a, \infty]$.

Proof. Consider the following Lyapunov function candidate:

$$V = \frac{1}{2}[\dot{e} + f(e) - ae]^2 + (kh_2 - a)\int_0^e f(e)de \tag{41}$$

The function V in Eq. (41) is an extension of the Lyapunov function candidate of Eq. (36) which was derived based on the *Liénard variable*, as discussed in Sec. 4.1. The function V is continuously differentiable, positive definite and radially unbounded. Taking its derivative along the trajectories of Eq. (40), we get

$$\begin{aligned}\dot{V} &= (\dot{e} + f(e) - ae)\left(\ddot{e} + \frac{df}{de} - a\dot{e}\right) + (kh_2 - a)f(e)\dot{e}\\ &= -(kh_2 - a)f^2(e) + a(kh_2 - a)f(e)e\\ &= -(kh_2 - a)f(e)[f(e) - ae]\end{aligned} \tag{42}$$

If $a \leq 0$ then the term $f(e)[f(e) - ae] > 0\,\forall\, e \neq 0$ and it is 0 only when $e = 0$. Hence, if $a \leq 0$ then $\dot{V} \leq 0$. The set $\dot{V} = 0$ is satisfied identically only by $e = \dot{e} = 0$. Since the above conditions are true globally, applying the Barbashin and Krasovskii theorem [8], we conclude that the origin $e = \dot{e} = 0$ is globally asymptotically stable.

For $a > 0$, the term $f(e)[f(e) - ae] > 0 \forall f(e) \in [a, \infty]$ and it is 0 only when $e = 0$. Hence, if this sector condition is satisfied then $\dot{V} \leq 0$. Applying the Barbashin and Krasovskii theorem as above, we therefore conclude that the origin $e = \dot{e} = 0$ is globally asymptotically stable under the aforementioned sector condition. ■

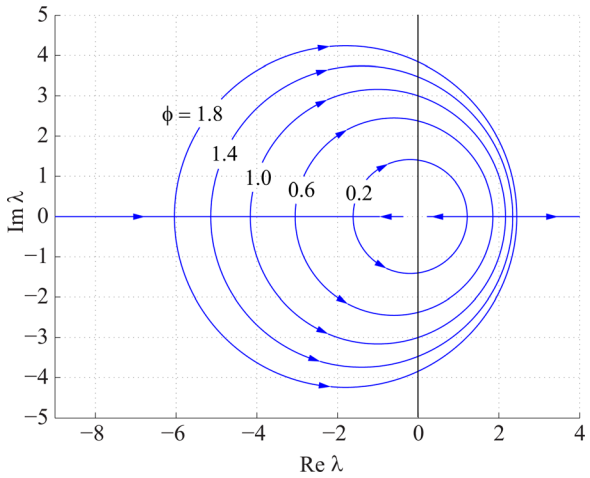

Fig. 7 Variation OF $\lambda_{1,2}$ with *a*, indicating Hopf bifurcation

By directly using the Liénard's theorem, Theorem 1, the following gives sufficient conditions for the existence of a unique and stable limit cycle for the feedback system of Fig. 6:

THEOREM 4. *Consider the feedback system of Fig. 6 where k is chosen such that* $(kh_2 - a) > 0$. *Let the unknown nonlinear function* $f(y,r) = -f(e)$ *satisfy* $f(0) = 0$, $ef(e) > 0 \forall e \neq 0$. *Further, let f(e) be a class* $\mathcal{K}_\infty$ *odd-function. Then, if* $a > 0$, *there exists a unique and stable limit cycle around the equilibrium* $\dot{e} = e = 0$ *if* $f(e) = ae$ *has a single positive root at* $e = e_0$.

Proof. We will prove this result by simply applying Theorem 1. We first note that in Eq. (40), the functions $((df/de) - a)$ and $(kh_2 - a)f(e)$ correspond to functions $p(\mu)$ and $q(\mu)$, respectively, in the general Liénard equation of Eq. (31). Since $f(e)$ is an odd function, $((df/de) - a)$ is an even function, and $(kh_2 - a)f(e)$ is odd. Furthermore, since $f(e)$ lies in the first and third quadrant and $(kh_2 - a) > 0$, $e(kh_2 - a)f(e) > 0 \forall e \neq 0$. Thus, condition 1 of Theorem 1 is satisfied. Next we consider the requirements of condition 2. Note that $\int_0^\infty (kh_2 - a)f(e)de \to \infty$ as $e \to \infty$ since $ef(e) > 0 \forall e \neq 0$. Furthermore,

$$\int_0^\infty \left(\frac{df}{de} - a\right) de = f(e) - ae \to \infty \quad \text{since} \quad f(e) > ae \forall e > e_0 \tag{43}$$

Thus, condition 2 is satisfied, and condition 3 is also satisfied since $ef(e) > 0 \forall e \neq 0$, and $f(e)$ is a class $\mathcal{K}_\infty$ odd-function with a single positive root of $f(e) = ae$ at $e = e_0$. Hence, the feedback system of Fig. 6 has a unique and stable limit-cycle around the origin $\dot{e} = e = 0$. ■

We note that the results of Theorems 3 and 4 refer to the generalized system in Fig. 6. The driver and driven equations of Fig. 6 are generic, since the driven equation is a linear first-order equation and the driver nonlinearity is a passive memoryless function. Also, the control law is a simple state-feedback. Hence, the results of Theorems 3 and 4 are applicable whenever this structure is satisfied. We also note that the problem of existence of limit cycle could potentially be studied using the *Describing Function* method [18]. However, Theorem 4 gives a sufficient condition, which is not guaranteed by describing functions. Finally, noting the transition from stable equilibrium in Theorem 3 to limit cycle in Theorem 4, we can infer the presence of *Hopf bifurcation* generated by the parameter *a* in Eq. (40) [10]. This can be verified by linearizing Eq. (40) about its equilibrium at the origin $\dot{e} = e = 0$. Assuming that the linearized approximation of $f(e)$ around the origin is $f(e) = \phi e$, $\phi > 0$, the linearized equation would be

$$\ddot{e} + (\phi - a)\dot{e} + (kh_2 - a)\phi e = 0, \quad \text{where} \quad (kh_2 - a) > 0 \tag{44}$$

The eigenvalues of this equation are at

$$\lambda_{1,2} = \frac{-(\phi - a) \pm \sqrt{(\phi - a)^2 - 4(kh_2 - a)\phi}}{2} \tag{45}$$

In Eq. (45), we note that $\left[(\phi - a)^2 - 4(kh_2 - a)\phi\right] \leq (\phi - a)^2$ since $4(kh_2 - a)\phi > 0$. Hence, if $a < \phi$, both eigenvalues will be stable. When $a = \phi$, the roots will be complex conjugates, located at $\lambda_{1,2} = \pm j\sqrt{(kh_2 - a)\phi}$. When $a > \phi$, we can similarly see that both eigenvalues will be unstable. The evolution of $\lambda_{1,2}$ with change in parameter *a* for different values of ϕ, is shown in Fig. 7. The plots are generated with $kh_2 = 10$. On each of the contours, the arrows represent direction of increasing value of *a*, while satisfying $(kh_2 - a) > 0$. For each value of ϕ in Fig. 7, the transition of $\lambda_{1,2}$ to the right-half plane occurs at $a = \phi$. The transition causes a *supercritical Hopf bifurcation*, indicating a limit cycle around the origin $\dot{e} = e = 0$. We end this section by noting that the existence of a limit cycle, under the conditions of Theorem 4, can be intuitively predicted. The conditions of Theorem 4, when valid, produces a damping in Eq. (44) that is negative for $e < e_0$ and positive otherwise. This creates an unstable equilibrium at $e = \dot{e} = 0$ but a stable limit cycle around it.

4.3 Simulations. We provide simulations in support of the results of Theorems 3 and 4. For verifying Theorem 3, we consider in Fig. 6, $a = 1.5$, and $kh_2 = 2.5$. The function $f(e)$ is constructed as $f(e) = \text{sign}(e)e^2 + 2e$. The function $f(e)$ is plotted in Fig. 8(*a*). We note that $f(0) = 0$, $ef(e) > 0 \forall e \neq 0$ and $f(e) \in [1.5, \infty]$. Hence, the equilibrium $\dot{e} = e = 0$ must be a globally asymptotically stable equilibrium. This is verified in Fig. 8(*b*). To verify Theorem 4, we consider $a = 4$ and choose $kh_2 = 5$. The latter choice is just to ensure $(kh_2 - a) > 0$ and any other number greater than four would suffice. Note that $f(e)$ is a class $\mathcal{K}_\infty$ odd-function, as required in Theorem 4. We also note from Fig. 8(*a*) that indeed $f(e) = 4e$ has a single positive root at $e = 2$. Thus, there must be a unique, stable limit cycle around the equilibrium $\dot{e} = e = 0$. This is verified in Fig. 8(*c*).

5 Stability Analysis Under Parameter Uncertainty

So far, we have assumed that the controller has accurate knowledge of the values of parameters h_1 and h_2, appearing in the

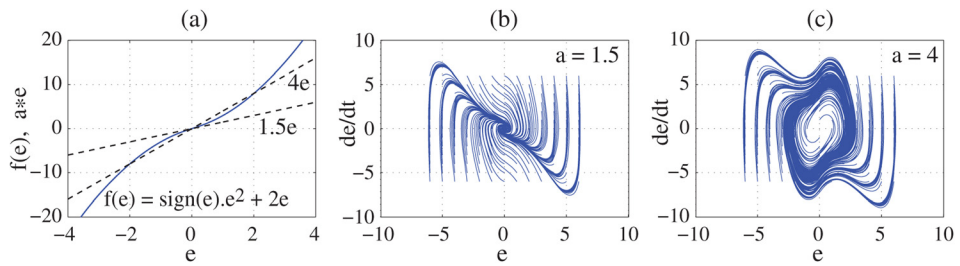

Fig. 8 Simulations to verify Theorems 3 and 4

dynamic equation of the driven system in Fig. 3. This is evident also from the control law of Eq. (13). We will now treat h_1 and h_2 as unknown parameters and modify the control law to incorporate robustness to parametric uncertainty. We note here that this extension will only be briefly studied in this paper, as the focus of this work are the results in Secs. 2–4.

5.1 Robustness Via Integral Action/Parameter Adaptation. Consider the feedback system of Fig. 3. Since h_1 and h_2 will now be treated as unknowns, the estimate of the combined parameter (h_1/h_2) is used in the control law, as shown below

$$r = -\hat{\beta} - kx, \quad k > 0, \quad \beta \triangleq \frac{h_1}{h_2} \tag{46}$$

where $\hat{\beta}$ represents the estimate of β. We define the estimation error

$$\mathcal{E} \triangleq (\beta - \hat{\beta}) \tag{47}$$

We propose the following integral update law for parameter estimation:

$$\dot{\mathcal{E}} = -\dot{\hat{\beta}} = -\gamma x \Rightarrow \mathcal{E} - \mathcal{E}_0 = -\gamma \int_0^t x\,dt, \quad \gamma > 0 \tag{48}$$

From Eqs. (10), (12), and (46)–(48) and noting that $e = (y - r)$, we deduce the following:

$$\dot{x} = h_2(\mathcal{E} + e - kx) = h_2 v, \quad v \triangleq \mathcal{E} + e - kx \tag{49}$$

and

$$\dot{e} = -f(e) + \gamma x + kh_2 v \tag{50}$$

Combining Eqs. (49) and (50), we obtain

$$\ddot{e} + \frac{df}{de}\dot{e} + kh_2 f(e) = -\gamma h_2 \int_0^t f(e)\,dt \tag{51}$$

Section 5.2 will analyze the stability of this closed-loop equation. Note that Eq. (48) is designed to make the resulting homogeneous equation in x stable. This can be seen from differentiating Eq. (49) with respect to time and substituting for $\dot{\mathcal{E}}$ from Eq. (48), which yields

$$\ddot{x} + kh_2\dot{x} + \gamma h_2 x = h_2\,\dot{e} \tag{52}$$

It is worth mentioning that the parameter estimation law of Eq. (48) could also be derived using *adaptive control* [18].

5.2 Stability Analysis. Comparing Eqs. (26) and (51), we see the addition of integral action to account for parameter uncertainty. This causes the closed-loop dynamics to be of third-order instead of second. By defining the variable $z = \int_0^t f(e)dt$, Eq. (51) can be expressed as

$$\dddot{e} + \frac{df}{de}\ddot{e} + kh_2 f(e) = -\gamma h_2 z, \quad \dot{z} = f(e), \quad \text{with} \quad z(0) = 0 \tag{53}$$

Since the function $f(e)$ is a passive memoryless function, the above system has a unique equilibrium at the origin $\dot{e} = e = z = 0$. We next analyze local stability of this origin, using linearization. Assuming that the linearized approximation of $f(e)$ around the origin is $f(e) = \phi e$, $\phi > 0$, we have from Eq. (53)

$$\dddot{e} + \phi\ddot{e} + kh_2\phi\dot{e} + \gamma h_2\phi e = -\gamma h_2 \int_0^t \phi e dt \Rightarrow \dddot{e} + \phi\ddot{e} + kh_2\phi\dot{e} + \gamma h_2\phi e = 0 \tag{54}$$

Using *Routh's Stability Criterion* [20], it can be shown that the necessary and sufficient condition for stability of the equilibrium $\dot{e} = e = z = 0$ for small perturbations is

$$k\phi > \gamma \tag{55}$$

Further analysis can be conducted to study the performance of the robust controller discussed in this section. Concepts of absolute stability, describing functions or bifurcations can potentially be applied. The generalization of Eq. (38) could also lead to interesting results for the robust control scenario, similar to the ones derived in Sec. 4.2. Furthermore, the third-order dynamics of Eq. (53) may also admit a strange attractor [10], under additional conditions. However, the focus of this work has been on Liénard systems, which are second-order, and their applications to stability analysis under unknown nonlinearities. Hence, the aforementioned extensions to incorporate parametric, albeit important, is not covered in this work in further details. In Sec. 5.3, we present simulations and results from Hardware-In-the-Loop (HIL) tests, to demonstrate the validity of the results of this section. We end this section with the following remark:

Remark 1. If $h_1 = 0$, then parameter uncertainty of h_2 need not be incorporated since, in that scenario, $\hat{\beta} = 0$. Hence, the integral control will not be necessary if $h_1 = 0$, and all results of Secs. 3 and 4 will be applicable.

5.3 Simulations and Experiments. To confirm the stability criterion of Eq. (55), simulations are done with a detailed model of a steam-reformer based SOFC system developed in Ref. [11]. The DC/DC converters C_1 and C_2, see Fig. 1, are modeled as static power conversion devices with efficiencies η_1 and η_2, respectively. Equation (1) is always satisfied within the model, thereby implementing power conservation in the hybrid energy system. Other important parameters are $\mathcal{N}_{\text{cell}} = 50$, $k_c = 0.55$, $V_L = 24\,\text{V}$, $U_{\text{ss}} = 80\%$, $S_t = 0.8$, $C = 250\,\text{F}$, $V_{\max} = 16.2\,\text{V}$, and $\eta_1 = \eta_2 = 0.85$. The simulation uses a constant load current

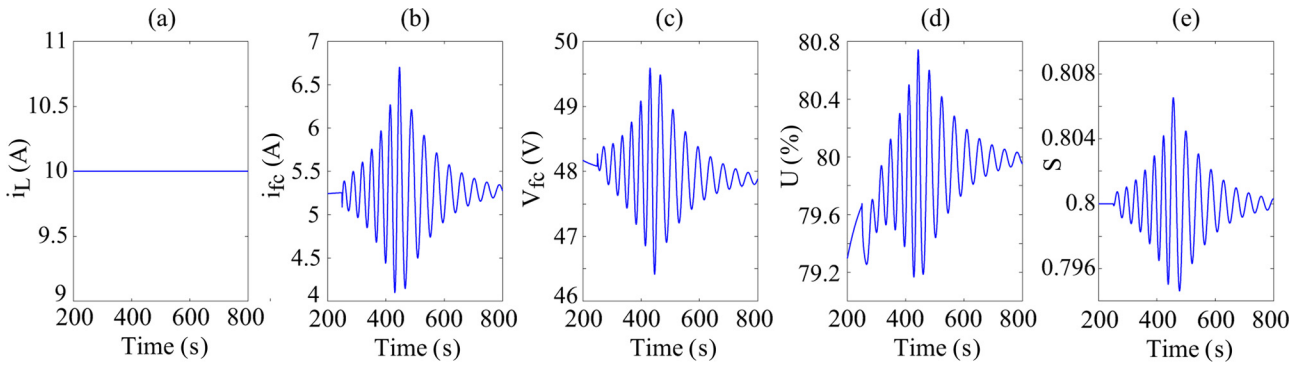

Fig. 9 Simulation verifying the stability result of Eq. (55)

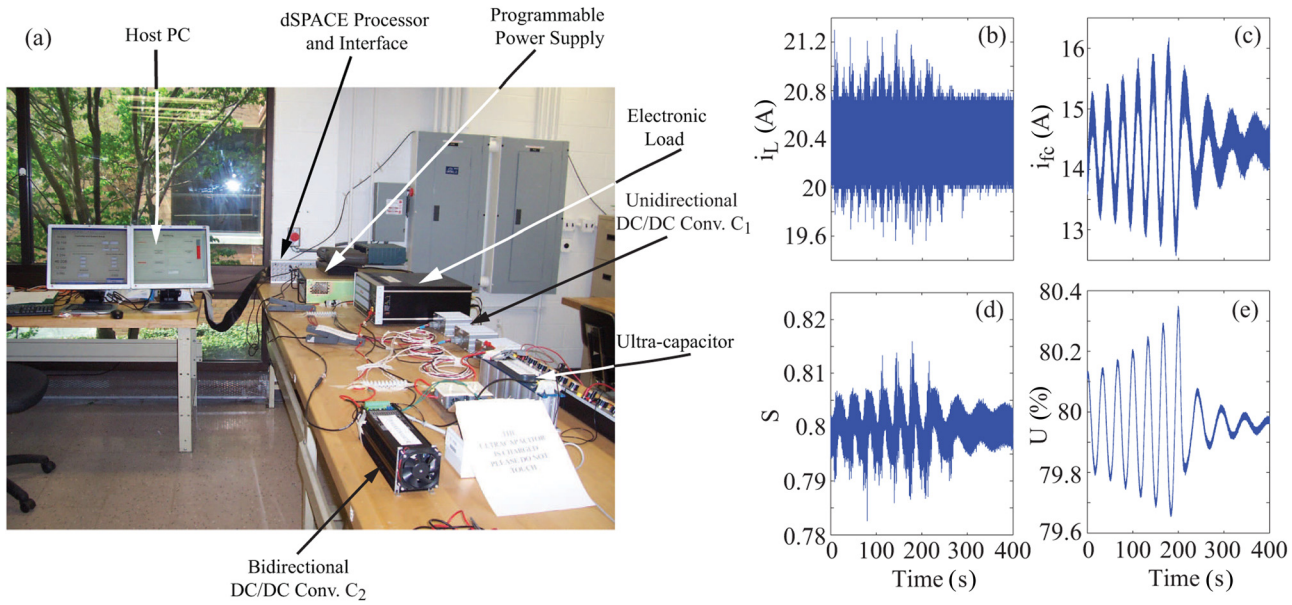

Fig. 10 HIL test stand and experimental results

$i_L = 10$ A. The parameter $\beta = h_1/h_2 = V_L i_L/(\eta_1 V_{\text{fc}})$ is given the initial estimate $\hat{\beta}(0) = 24 \cdot 10/(0.9 \cdot 48) = 5.56$. The FSS is modeled as $\dot{N}_f(s)/\dot{N}_{f,d}(s) = 1/(2s+1)$, which effectively means $\frac{d\, i_{\text{fc}}}{dt} = -0.5(i_{\text{fc}} - i_{\text{fc},d}) \Rightarrow \dot{y} = -0.5e$. Hence, $f(e) = 0.5e$, $\phi = 0.5$, and the dynamics are treated as unknown by the controller. Also a value of $k = 70$ was chosen so that the equilibrium is stable for $\gamma < 35$ and unstable otherwise.

Figure 9 shows the system response to a constant input of $i_L = 10A$. The simulation was run with $\gamma = 46$ for $t < 450$ s and $\gamma = 23$ for $t \geq 450$ s. Use of parameter estimation $\hat{\beta}$ is off initially and switched on at $t = 250$ s. Upon switching on, $\gamma = 46$ produces an unstable equilibrium and hence the divergence of trajectories over time is seen. The equilibrium stabilizes for $t > 450$ s when γ is switched to a value below the threshold of 35. The two values of γ were sufficiently separated from the threshold with the understanding that the parameters assumed constant are actually slowly time-varying and hence Eq. (55) should be interpreted as an estimate. In Fig. 9(*e*), S represents the SOC and $x = S - S_t = S - 0.8$. Thus equilibrium corresponds to $S = 0.8$. Also, note the relatively small deviations of U around $U_{\text{ss}} = 80\%$ in Fig. 9(*d*). This is due to internal current regulation in the fuel cell. Also, note that $i_L = 10A$ throughout, Fig. 9(*a*). This confirms that the instability is not due to external conditions but induced by the interaction of the controller and FSS under improper choice of the estimation gain γ.

We next show the experimental results form a HIL setup. The HIL system is shown in Fig. 10(*a*). The SOFC model of Ref. [11] is emulated using a dSPACE DS1103PPC real-time operating system and an SGA series Sorensen DC programmable power supply. The emulated fuel cell is connected to an electronic load using an SD-1000L-24 unidirectional DC/DC converter from Mean Well. A 16.2 V series BMOD0250-E016 ultracapacitor from Maxwell Technologies with a 250 F capacitance is connected in parallel to the fuel cell. It is interfaced using a DC5050F-SU bidirectional DC/DC converter from Zahn Electronics, Inc. A Sorensen 1.8 kW SLH series DC programmable electronic load is used for power draw. Further details pertaining to this system can be found in Ref. [6]. The overall connectivity follows the schematic of Fig. 1.

Experiments were conducted on the HIL setup with $V_L = 24$ V, $U_{\text{ss}} = 80\%$, target SOC $S_t = 0.8$, ultracapacitor $C = 250$ F and $V_{\max} = 16.2$ V. The initial parameter estimates $\hat{\beta}(0) = 5.56$, as in the simulation run. The FSS model is also the same as in the simulations, and is treated as unknown by the controller. Also, $k = 70$ for the HIL tests, which implies a stability-threshold at $\gamma = 35$. In the plots, $t = 0$ s is the start of parameter estimation and data capture. Figures 10(*b*)–10(*e*) show results for $\gamma = 50$ when $t < 200$ s and $\gamma = 20$ when $t \geq 200$ s. The results indicate an unstable equilibrium for $t < 200$ s which becomes stable when the stability criterion is satisfied, as expected. The γ values are separated enough to provide for a buffer to the time-varying parameter β in the hardware setup. Although there is error induced in various stages of the process, the general result of Eq. (55) provides a relatively good approximation. We also note that the plots were zoomed-in to show the transients and hence the noise appears to be considerable. The noise-to-signal ratio is <5% in all the plots. The control design and implementation were based on Assumption 2 of Sec. 2.2, i.e., h_1 and h_2 are constants. The results of this section show that the stability criterion of Eq. (55), based on this assumption, is valid in predicting the onset of instability reasonable accuracy. The validity is because $\dot{h}_1$ and $\dot{h}_2$ are small in magnitude. Using the estimated variations of η_1 and η_2 from Ref. [7], and the worst case variations of V_{fc} and S from Figs. 9 and 10, we can verify that $\dot{h}_1$ and $\dot{h}_2$ are both of $O(10^{-6})$. Further, $\dot{\beta}$ is $O(10^{-2})$ and is approximately an order of magnitude lower than $k\dot{x}$ in simulations and experiments. Thus, from data and Eq. (13), we note that $\dot{r}$ is largely governed by $k\dot{x}$.

6 Conclusions

The work presented in this paper originates from the problem of controlling an ultracapacitor's SOC in a hybrid SOFC system, by modulating the fuel cell's delivered power. The challenge is the unknown nonlinear-dynamics of the FSS prevent the controller from compensating the ultracapacitor in a deterministic manner. Upon generalization, a theoretical problem is formulated where the closed-loop stability of a plant is studied for different classes of nonlinear functions. The unknown nonlinearity is expressed in a cascaded manner in the plant dynamics, and this allows application of conventional absolute stability results. However, we show that more definitive and comprehensive stability results are possible if the problem is analyzed from the perspective of nonlinear dynamics. In particular, the generalized problem is shown to conform to a class of Liénard equations. Liénard equations are well-studied and by utilizing their established analytical

background, conditions for asymptotic stability, limit cycles and conditions for transitioning between them are derived. The analytical framework can be extended to the scenario where parameter uncertainty must be incorporated. In this regard, some preliminary results are also derived. Simulations and some HIL experiments are provided to demonstrate the efficacy of the theory developed.

Acknowledgment

This work was supported in part by the Office of Naval Research under Grant No. N000140910272 and in part by the National Science Foundation under Grant No. 1158845.

References

[1] Larminie, J., and Dicks, A., 2003, *Fuel Cell Systems Explained*, Wiley, Chichester, UK.
[2] Lazzaretto, A., Toffolo, A., and Zanon, F., 2004, "Parameter Setting for a Tubular SOFC Simulation Model," ASME J. Energy Resour. Technol., **126**(1), pp. 40–46.
[3] Sedghisigarchi, K., and Feliachi, A., 2002, "Control of Grid-Connected Fuel Cell Power Plant for Transient Stability Enhancement," IEEE Power Engineering Society Winter Meeting, Vol. 1, pp. 383–388, Cat. No.02CH37309.
[4] Campanari, S., 2001, "Thermodynamic Model and Parametric Analysis of a Tubular SOFC Module," J. Power Sources, **92**(1–2), pp. 26–34.
[5] Das, T., and Weisman, R., 2009, "A Feedback Based Load Shaping Strategy for Fuel Utilization Control in SOFC Systems," American Control Conference (ACC-09), St. Louis, MO, June 10–12, pp. 2767–2772.
[6] Allag, T., and Das, T., 2012, "Robust Nonlinear Control of Solid Oxide Fuel Cell Ultra-Capacitor Hybrid Systems," IEEE Trans. Control Syst. Technol., **20**(1), pp. 1–10.
[7] Das, T., and Snyder, S., 2013, "Adaptive Control of a Solid Oxide Fuel Cell Ultra-Capacitor Hybrid System," IEEE Trans. Control Syst. Technol., **21**(2), pp. 372–383.
[8] Khalil, H., 2002, *Nonlinear Systems*, 3rd ed., Prentice-Hall, Inc., Upper Saddle River, NJ.
[9] Davis, H. T., 2010, *Introduction to Nonlinear Differential and Integral Equations*, Dover Publications, Inc., New York.
[10] Strogatz, S. H., 2001, *Nonlinear Dynamics and Chaos*, 1st ed., Westview Press, Cambridge, MA.
[11] Das, T., Narayanan, S., and Mukherjee, R., 2010, "Steady-State and Transient Analysis of a Steam-Reformer Based Solid Oxide Fuel Cell System," ASME J. Fuel Cell Sci. Technol., **7**(1), p. 011022.
[12] Sedghisigarchi, K., and Feliachi, A., 2002, "Control of Grid-Connected Fuel Cell Power Plant for Transient Stability Enhancement," IEEE Power Engineering Society Transmission and Distribution Conference, Vol. 1, pp. 383–388.
[13] Stiller, C., Thorud, B., Bolland, O., Kandepu, R., and Imsland, L., 2006, "Control Strategy for a Solid Oxide Fuel Cell and Gas Turbine Hybrid System," J. Power Sources, **158**(1), pp. 303–315.
[14] Nehrir, M. H., and Wang, C., 2006, *Modeling and Control of Fuel Cells–Distributed Generation Applications*, Wiley, Hoboken, NJ.
[15] Murshed, A. M., Huang, B., and Nandakumar, K., 2010, "Estimation and Control of Solid Oxide Fuel Cell System," Comput. Chem. Eng., **34**(1), pp. 96–111.
[16] Gaynor, R., Mueller, F., Jabbari, F., and Brouwer, J., 2008, "On Control Concepts to Prevent Fuel Starvation in Solid Oxide Fuel Cells," J. Power Sources, **180**(1), pp. 330–342.
[17] Sastry, S., 1999, *Nonlinear Systems: Analysis, Stability and Control*, Springer-Verlag, New York.
[18] Slotine, J., and Weiping, L., 1991, *Applied Nonlinear Control*, Prentice-Hall, Inc., Upper Saddle River, NJ.
[19] Vidyasagar, M., 2002, *Nonlinear Systems Analysis*, 2nd ed., Society for Industrial and Applied Mathematics, Philadelphia, PA.
[20] Franklin, G. F., Powell, J. D., and Emami-Naeini, A., 2014, *Feedback Control of Dynamic Systems*, 7th ed. Prentice Hall, Upper Saddle River, NJ.